Urban Climate 39 (2021) 100961

Contents lists available at ScienceDirect

Urban Climate

journal homepage: www.elsevier.com/locate/uclim

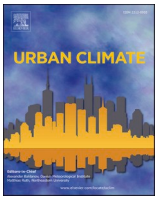

High resolution modeling of the impact of urbanization and green infrastructure on the water and energy balance

Rebecca Wiegels [a], Fernando Chapa [b], Jochen Hack [b,*]

[a] Technical University of Darmstadt, Department of Civil and Environmental Engineering, Franziska-Braun-Str. 7, 64287 Darmstadt, Germany
[b] Technical University of Darmstadt, Institute of Applied Geosciences, Section of Ecological Engineering, Research Group SEE-URBAN-WATER, Schnittspahnstr. 9, 64287 Darmstadt, Germany

ARTICLE INFO

Keywords:
Green infrastructure
Water balance
SUEWS
Energy balance
Bowen ratio
Urbanization

ABSTRACT

Sealed surfaces in urban areas change the water and energy balance resulting in decreased evapotranspiration and infiltration, magnified stormwater runoff, and sensible heat fluxes. Urban Green Infrastructures (UGI) are implemented to reverse such effects. This study examines the potential of a high-resolution grid-based model to show the impact of different degrees of urban land cover. The study area was divided into 52 cells and cells were categorized into four urban degrees of urbanization. Two scenarios were considered to represent the existing conditions of a study area in the Great Metropolitan Area of Costa Rica and the effects derived from the implementation of UGI. The software Surface Urban Energy and Water Balance Scheme (SUEWS) was employed to simulate both scenarios and compare them by using the Bowen ratio (β) as an indicator of changes in the energy balance. The results show a reduction of β associated with the spatial distribution of the cells with different degrees of urbanization, even in the cells where no changes were considered. Applying the SUEWS approach based on high-resolved land cover classes distribution enables a more detailed understanding of micro-climatic benefits of UGI in high-density urban areas and may result in additional insights for decision-making.

1. Introduction

Benefits of Green Infrastructures (GI) in urban areas - also known as Sustainable Urban Drainage Systems, Low Impact Development, or Water Sensitive Urban Design (Fletcher et al., 2015) - are largely promoted by policy-makers (EPA, 2020; European Communities, 2001) and scientists (Hansen et al., 2019; Meerow, 2020). By connecting or modifying existing urban green spaces or through the creation of new greenery elements, GI attempts to increase biodiversity and improve human well-being (European Commission, 2013). The latter is pursued by mitigating the negative impacts of urbanization on the hydrological and energy balance.

GI have been evaluated and tested concerning their hydrological performance in surface runoff reduction (Ahiablame et al., 2012; Chui et al., 2016; Dietz, 2007; Dietz and Clausen, 2008; Juan et al., 2017) and several numerical models have been developed (Elliott and Trowsdale, 2007; Jayasooriya and Ng, 2014; Kaykhosravi et al., 2018). Both freely available and commercial models are employed in practice and research to assess runoff reduction and water quality impacts due to GI implementation (Dietz and Clausen, 2008; Elliott and Trowsdale, 2007; Jayasooriya and Ng, 2014; Li et al., 2019; Luan et al., 2019).

* Corresponding author.
E-mail addresses: rebecca.wiegels@stud.tu-darmstadt.de (R. Wiegels), chapa@geo.tu-darmstadt.de (F. Chapa), hack@geo.tu-darmstadt.de (J. Hack).

https://doi.org/10.1016/j.uclim.2021.100961
Received 21 May 2021; Received in revised form 8 July 2021; Accepted 14 August 2021
Available online 18 August 2021

Lumped conceptual models, that summarize bio-physical processes in large spatial units such as subcatchments, are typically used for the hydrological assessment of GI (Elliott and Trowsdale, 2007; Jayasooriya and Ng, 2014; Kaykhosravi et al., 2018). However, these models are often unable to estimate spatially discrete changes in the hydrological and energy balance resulting from GI implementation (Kumar et al., 2021). The hydrological efficiency of green infrastructure at the catchment or subcatchment scale has been reported in several studies using lumped conceptual models (Göbel et al., 2004; Joyce et al., 2017; Stewart et al., 2017; Zhang and Chui, 2017), but without reporting spatially discrete changes in the hydrological and energy balance resulting from exact site of GI implementation. Thus, on-site benefits of GI, such as local microclimate regulation, cannot be assessed (Ketabchy et al., 2019). Potential benefits that such assessment can have for densely urbanized areas are not capitalized on.

Conversely, distributed grid-based water and energy balance models enable spatially explicit assessments of on-site benefits from microclimate regulation (Lindberg et al., 2018a). Several empirical studies could demonstrate that distributed grid-based models enable to model spatially discrete changes in the hydrological and energy balance resulting from land cover changes (Kokkonen et al., 2019; Mitchell et al., 2008; Ward et al., 2016). However, typical Urban Green Infrastructure (UGI) elements (e.g., bioretention cells, permeable pavement, swales, stormwater trees, constructed wetlands) that are commonly simulated hydrologically in conceptual models, have not yet been evaluated with spatially distributed models concerning their on-site benefits of microclimate regulation due to small scale changes in the hydrological and energetic balance.

The objective of this study to use a distributed grid-based model which enabled a detailed spatial representation of fragmented and densely urbanized areas and flexible simulation of UGI structures. This approach was chosen to explicitly evaluate the on-site benefits of microclimate regulation through UGI and thereby to show to what degree these benefits can be achieved. The Surface Urban Energy and Water Balance Scheme (SUEWS) was applied in this study to quantify the mitigation effect of a fieldwork-based UGI implementation strategy. The study focused on the process of evapotranspiration as a linking component for the hydrological and the energy balance and sensible heat flux.

Contrary to other models commonly used to simulate UGI, such as the Storm Water Management Model (SWMM), SUEWS does not enable explicit simulation of UGI elements. This restricts the level of detail of interconnected drainage elements (e.g. technical aspects: lining, overflow structures, or different subsoil layer properties) regarding their hydraulic and hydrological functioning, such as storage, release, and overflow. But it also restricts other related functions such as infiltration and evapotranspiration. However, an advantage of SUEWS compared to hydraulic or hydrological models is the explicit and detailed modeling of the cell's energy and water balance. This enables one to estimate the impact that UGI implementation on surface fraction change by using SUEWS.

An urban residential area in the Greater Metropolitan Area of San José, Costa Rica, where UGI elements are being developed and experimentally implemented as part of the ongoing SEE-URBAN-WATER[1] research project (Chapa et al., 2020; Neumann and Hack, 2019; Pérez Rubi and Hack, 2021) was used as a case study. The study area was chosen because UGI are empirically designed and tested in this area and detailed information regarding the implementation potential (location, types, and geometries) were available from previous studies (Fluhrer et al., 2021). With the use of a high spatial resolution land cover classification, grid cells of different degrees of urbanization were identified and modeled as the status quo. Afterward, suitable sites were modified to represent an implementation scenario of UGI. The results were evaluated spatially concerning cells of differing degrees of urbanization, comparing the status quo and the possible impact of UGI implementation. The study provides important conceptual insights on how small-scale urban GI elements can be represented in a highly resolved distributed grid-based model and practice-based information of the on-site benefits of UGI.

2. Materials and methods

2.1. Study area

The neighborhood case study area is situated in a rapidly developing area where commercial and industrial activities take place nearby. The site has an area of around 0.5 km^2 and is bounded by a river (south), one municipal street (north), abandoned land (east), and one of the most transited highways in the country (west). The average annual precipitation is 2000 mm, with most of the rainfall falling during the wet season (June–October). Temperature varies in a range between 20° and 30 °C throughout the year, with a slight increase during March and April (Towsif Khan et al., 2020).

Fig. 1 depicts an overview of the location and urbanization degree of the study area. All the streets are paved, including sidewalks. Variation in housing reflects variation in economic success. Houses are typically built with reinforced concrete walls and either metal sheets or tile roofs. The biggest and newest houses are situated on the northern side, where abundant green strips can be observed parallel to the sidewalks. Green spaces are scarce in more populated parts of the neighborhood, existing primarily in front and backyards. Small patches of trees remain in some vacant lots. Additional vegetation belongs to public playgrounds or bareland, especially along the riparian zone. As mandated by national law, this zone must have a minimum width of 10 m as a protection corridor. However, this measure is frequently violated due to the continuous erosion of the river banks, or land reclamation for urbanization (Chen et al., 2021).

[1] www.tu-darmstadt.de/see-urban-water

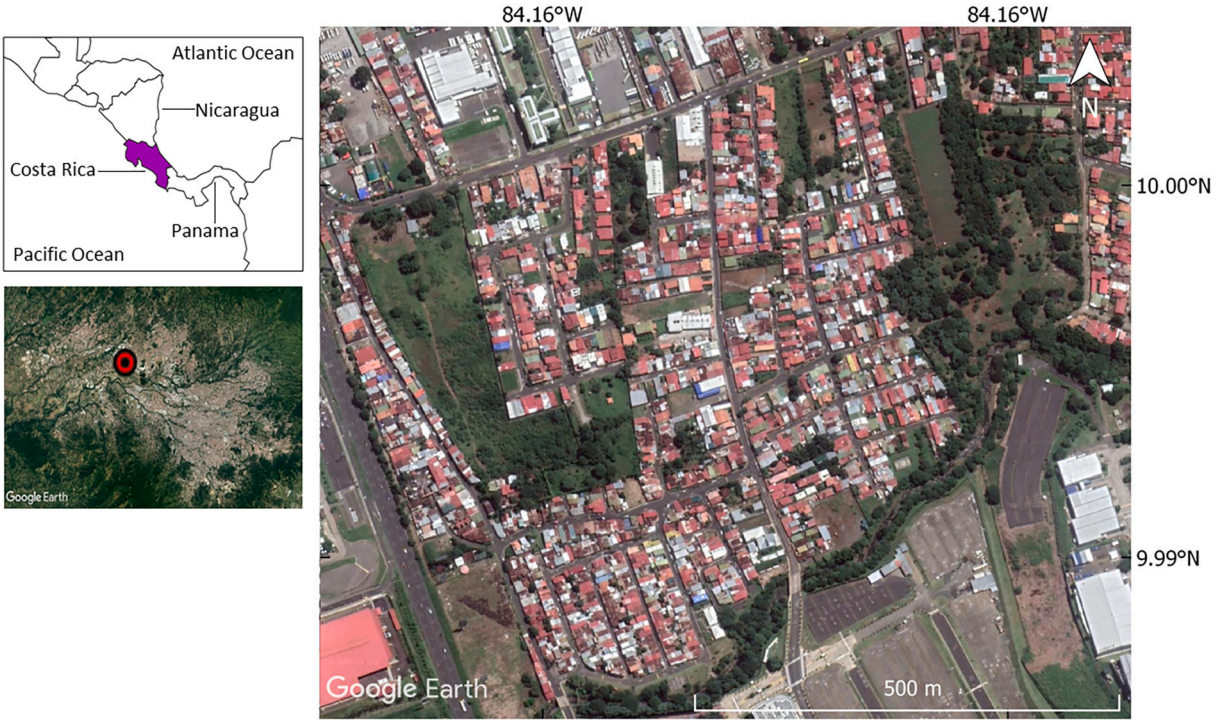

Fig. 1. Overview of the study site (right) located in the Greater Metropolitan Area (bottom left) in Costa Rica (top-left). Adapted from Google Earth.

2.2. Model description

This section describes the hydrological and energetic principles and parameters employed by the model SUEWS. The output of the model was used to evaluate the performance and spatial impact of implementing UGI elements in an urban neighborhood.

The model enables the simulation of the urban hydrological and energy balance at a wide range of spatial scales, including the neighborhood scale. Within an urban area, water is added either as rainfall (P), irrigation, or piped water (I). To determine the evapotranspiration (E), the runoff (R), and the change in storage (ΔS) SUEWS employs the urban hydrological balance proposed by Grimmond et al. (1986; see Eq. 1).

$$P + I = R + E + \Delta S \tag{1}$$

Based on the urban energy balance equation (Eq. 2) proposed by Oke (1978), the available energy is determined with hourly sub-calculations of the net all-wave radiation (Q*), the anthropogenic heat flux (Q_F), and net storage heat flux (ΔQ_S). In this study, Q* was simulated using the SUEWS sub-model Net All-Wave Parameterization scheme (NARP) (Loridan et al., 2011; Offerle et al., 2003) which requires short-wave radiation, relative humidity, and air temperature besides radiometric surface characteristics to model, if not observed, longwave radiation. The anthropogenic heat flux includes energy released from buildings, due to air conditioning or heating, cooking, transportation, and human metabolism (Ward et al., 2016). Based on the model recommendation, Q_F was simulated using an approach of Sailor and Vasireddy (2006a), based on the number of Cooling - and Heating Degree Days (CDD and HDD) per population density. ΔQ_S was defined using the Objective Hysteresis Model (OHM) incorporated in SUEWS, which includes the surface cover fraction for each surface type as well as OHM coefficients obtained from Grimmond (1998). The sensible heat flux (Q_H) is obtained in SUEWS as residues of the energy balance (Ward et al., 2016). The latent heat flux (Q_E) is obtained from the product of latent heat of vaporization (LV) and the flux of mass of Evapotranspiration (E) (Järvi et al., 2011).

$$Q^* + QF = QE + QH + \Delta QS \tag{2}$$

Surface and soil storage were employed to simulate the urban water balance. The surface storage, which can occur on any urban surface type (i.e., paved, buildings, deciduous trees/shrubs, evergreen trees/shrubs, grass, bare soil, water), and underneath soil storage (except under the water layer) were considered to calculate the output parameters of the hydrological balance.

A time-step of 5 min is employed in the model to calculate the wetness stage, representing the water content of each layer per cell according to a water balance per surface (Eq. 3a), and one stage per each soil underneath (Eq. 3b). In Eq. 3a, C_i represents the surface wetness stage of the i_{th} surface, calculated for a certain time-step t. C_i is dependent on precipitation (P), the water from a neighboring surface (R_{S2S}; S2S = surface to surface), water inflow from a neighboring grid cell (R_{G2G}: G2G = grid cell to grid cell) or irrigation (I). Water loss can occur either through evapotranspiration (E) or drainage (D).

$$C_i = C_{i,t-1} + \left(P_i + I_{e,i} + R_{G2G,i} + R_{S2S,i}\right) - \left(D_i + E_i\right) \quad (3a)$$

Surfaces are differentiated between impervious and pervious. Impervious surface allows drainage to connected surfaces (i.e. R_{S2S}), depending on specified hydrological connectivity and topographic characteristics of the site. Residues drainage water flows into a pipe network (R_{pipe}) until the capacity of the pipe is exceeded, then the excess water runs off above ground ($R_{AG,\ imp}$: AG, imp = above ground, impervious). Conversely, pervious surfaces drain partly as infiltration into the underlying soil layer ($R_{I,i}$: I = infiltration) until saturation exceeds either the soil capacity or precipitation intensity goes beyond 10 mm per 5 min. The latter is predefined in the model. Here, the drainage from pervious surfaces becomes (R_{pipe}) until it reaches its maximum capacity, turning consequently into above-ground runoff ($R_{AG,veg}$: AG, veg = above ground, vegetated).

Eq. 3b describes the amount of water within a soil layer. $C_{Soil,i}$ represents the state of soil storage, influenced by infiltration ($R_{I,i}$), by evapotranspiration (E_i), horizontal flow underground into a connected soil layer ($R_{BG,i2j}$: BG = below ground, from soil layer i to soil layer j), and is calculated according to Green and Ampt's equation (Green and Ampt, 1911) or as deep soil runoff (R_{DS}: DS = deep soil) when the soil storage exceeds its capacity. Since R_{DS} is disconnected from the grid system, it can be considered as deep infiltration leaving the model.

$$C_{soil,i} = C_{soil,i,t-1} + R_{I,i} - E_i - R_{BG,i2j} - R_{DS} \quad (3b)$$

The water flux transformed to evapotranspiration is simulated when the i_{th} surface above is dry ($C_i = 0$) as long as $C_{soil,i} > 0$. E_i is then calculated and subtracted from Eq. 3b. With below-ground runoff, which is not connected to a soil layer underneath, no drainage occurs. The water fluxes considered in this surface are solely surface-to-surface runoff and evapotranspiration.

Evapotranspiration is calculated for each surface using the Penman-Monteith equation modified for urban areas (Grimmond et al., 1991), where Q_E describes the turbulent heat flux, r_a is the aerodynamic resistance, r_s the surface resistance, ρ is the density of air, c_P the specific heat capacity of air at constant pressure, VPD the vapor pressure deficit, s the slope of the saturation vapor pressure curve, and γ the psychrometric constant.

$$Q_E = \frac{s(Q^* + Q_F - \Delta Q_s) + c_P \rho VPD / r_a}{s + \gamma(r_s / r_a)} \quad (4)$$

Consequently, evapotranspiration depends on the surface wetness state calculated as described throughout this section. For Eq. 4 the surface resistance r_s is redefined depending on the state of wetness. A value equal to zero is set to r_s when the surface is completely wet, which occurs when drainage exceeds the storage capacity of the surface. As soon as an impervious surface is completely dry ($C_i = 0$), evapotranspiration occurs on the surrounding pervious surfaces. Water is removed as evapotranspiration from the underneath soil layer when the pervious surface dries.

The SUEWS model calculates an hourly total runoff, the sum of pipe runoff and above ground runoff of impervious and pervious surfaces, and evapotranspiration from every 5-min update from previously described parameters.

A grid is employed in SUEWS to represent the modeling area. It enables the simulation of horizontal water flows between cells, and vertical water flows between the surface and soil layers within cells as described above. Fig. 2 illustrates those fluxes between cells and layers of one grid cell row. All horizontal flows between grid cells indicated in the figure are also modeled to parallel grid cell rows.

2.3. Model setup and data

The SUEWS model is an open-source program that can be accessed via the UMEP Plugin (Urban Multi-scale Environmental Predictor)(Lindberg et al., 2018b) in the geoinformation software QGIS or as a standalone model in Python (Sun and Grimmond, 2019). In this study, the model was run using the UMEP Plugin, version 3.12.1, released in SUEWS (v2019a) (Grimmond, 2020). To obtain evapotranspiration at each cell, data regarding shortwave radiation, precipitation, wind speed, relative humidity, air temperature, and

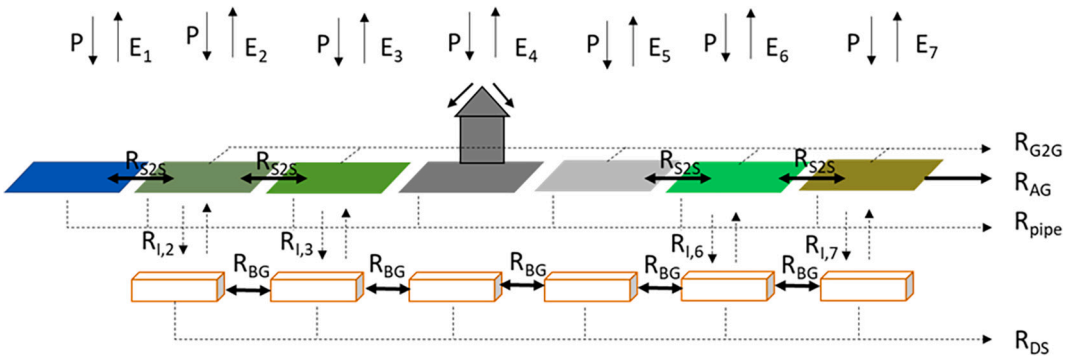

Fig. 2. Water scheme of SUEWS based on (Järvi et al., 2011) showing horizontal and vertical water fluxes: precipitation (P), evapotranspiration (E), and various types of runoff (R).The subscirpt numbers of E and R refer to the surface type, further explaination regarding the subscripts is given in the text.

pressure is required. This set of data was obtained from two meteorological stations, one located within the study area (see yellow cross in Fig. 3), and the second at a site approximately 7 km away.

The model was run from the 18th of October 2019 to the 16th of November 2019, a period with dry and rainy days. Table 1 summarises the statistical values for each meteorological parameter of the data set within a 60-min time step, obtained from measurements registered every 30 min (radiation) or every 15 min (wind, relative humidity, temperature, pressure, precipitation).

Site characteristics required in the model for a user-defined grid are population density, tree characteristics, and building characteristics. According to the developers, the model has been used based on grid cell sizes of 400 × 400 m and larger. For this study it was assumed that the model is also suitable for smaller grid cell sizes. The grid used is composed of fifty-two 100 × 100 m cells, which was the smallest grid size the model was able to process with the data used in this study. Fig. 3 shows the distribution of those cells in the study site that has a total area of 518,371 m^2.

The population density is a variable required in SUEWS to model the anthropogenic impact on the energy balance based on energy consumption. Since the direct anthropogenic impact on the local climate through heating or cooling was not the main focus in this study, an average population density for all grid cells based on the known overall population of the area was assumed for both model

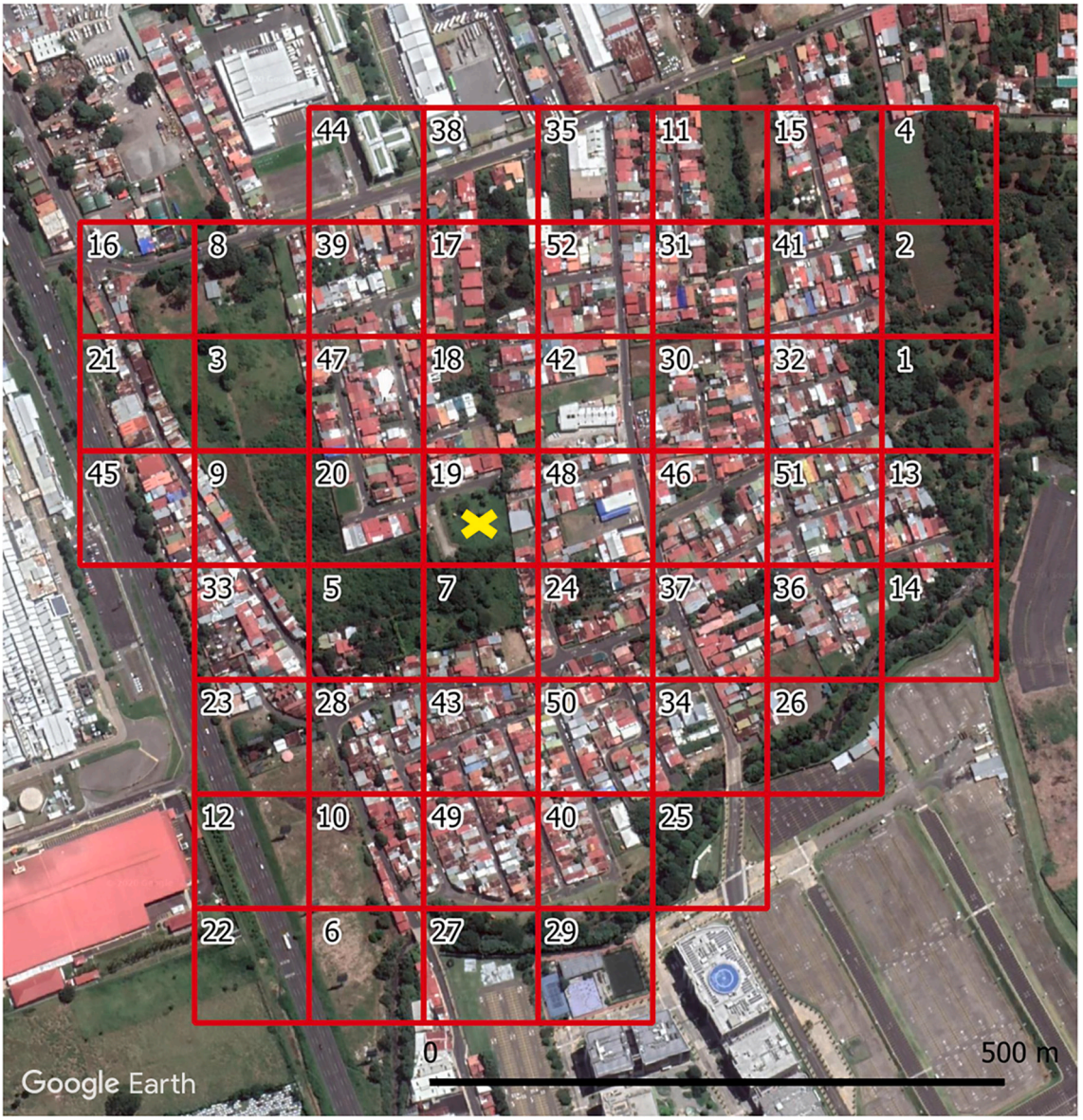

Fig. 3. Study site including modeling grid and grid cell numbers increasing with the degree of urbanization of cells. The yellow cross marks the location of the meteorological station. Google Earth image used for the high-resolution land cover classification is displayed in the background. (For interpretation of the references to colour in this figure legend, the reader is referred to the web version of this article.)

Table 1
Magnitude of meteorological values passed to SUEWS for both model set ups. The extent is represented by their statistical values: maximal value (max), median, minimum value (min) and the standard deviation of the respective data set (stand. Deviation).

	Unit	Max	Median	Min	Standard Deviation
Day (6 am – 5 pm)					
Wind	m/s	1.94	0.83	0.01	0.46
Relative Humidity	%	96	74	49	11
Temperature	°C	29.6	24.3	17.1	2.5
Pressure	kPa	91.30	90.81	90.37	0.19
Precipitation	mm/h	23.4	0.0	0.0	1.4
Radiation	W/m^2	1021	256	0	270
Night (6 pm – 5 am)					
Wind	m/s	1.94	0.42	0.01	0.45
Relative Humidity	%	96	88	66	7
Temperature	°C	23.6	20.3	17.1	1.2
Pressure	kPa	91.28	90.87	90.37	0.17
Precipitation	mm/h	1.8	0.0	0.0	0.1
Radiation	W/m^2	1	0	0	0

runs. The population density of 0.626 ha^{-1} (INEC, 2020) was assumed to be constant throughout the grid.

A tree height equal to 15 m (12 m for implemented stormwater trees as part of the UGI scenario) was adopted based on recommendations for urban tree selection within residential areas in Costa Rica (Curridabat, 2021). The mean building height was defined as 3 m based on field observations. Using those site characteristics a Digital Surface Model (DSM) and a Canopy Digital Surface Model (CDSM) were created using the pre-processor tool "Tree Generator" included in UMEP. Subsequently, the DSM and CDSM were employed to obtain the roughness parameters at each cell for calculation of evapotranspiration. That process employed the pre-processor tool "Morphmetric Calculator".

The land cover distribution within the entire study area was determined and quantified using satellite images from Google Earth Pro (approximate resolution: 1.3 m, date: 6th Jan. 2020) in the Semi-Automatic Classification Plugin (Version 6.4.2.), following the procedure described in Chapa et al. (2019). The pre-processor tool "Land Cover Fraction (Grid)" was subsequently used to obtain the percentage of land use at each cell. The resulting surface fractions for the total grid used for the status quo and UGI scenario model runs are presented in Table A.1 of Appendix A.

The initial soil moisture was initially set to 40%, based on the calculation of the average observational soil moisture data from the study area in October 2019, where three soil moisture sensors (ONS-S-SMC-M005) were installed at soil depths of 10, 45, and 80 cm. The initial leaf state, a model parameter that enables the representation of different seasons, was set to 100%. Default values such as surface conductance parameters and albedo, storage and drainage values for each surface type were used (Järvi et al., 2011).

2.4. Modeling urban scenarios

This section describes the three methodological steps applied to model urban effects on the hydrological and water balance for the status quo and the hypothetical UGI scenario.

2.4.1. Categorization of grid cells according to different degrees of urbanization

The degree of urbanization was determined by the land cover percentages, i.e. surface cover fractions, of a cell. In this study, urbanization is understood as a process of land cover transformation from perivous to impervious surfaces. A categorization was conducted based on the determination of land cover share (surface cover fraction) for each grid cell. The surface cover types of SUEWS were grouped into either urbanized (i.e. impervious surface types such as buildings and streets), and non-urbanized land cover (i.e. pervious surface such as evergreen and deciduous trees/shrubs, grass, bare soil, and water). Four categories were defined in proportion to the average value of the land cover shares (see Table 2).

This categorization of cells according to their degree of urbanization was used to evaluate the impact of the degree of urbanization on the hyrological and energy balance.

2.4.2. Simulation of UGI scenarios

Two simulation setups were developed to compare the impact of implementing UGI measures in the study area. The first simulation represents the current state of the study area, which is defined as the status quo. The second simulation represents the spatially explicit implementation of specific UGI measures: permeable pavement, stormwater trees, bioretention areas, swales, and constructed wetlands. This modeling scenario was developed based on field work in the study area and further analysis identifying potential sites for the different multi-functional UGI elements as part of the SEE-URBAN-WATER research project (Fluhrer et al., 2021). Specific local conditions (e.g. very few available green spaces, highly trafficked roads, distribution and characteristics of existing green spaces) were considered in developing this UGI implementation scenario. The resulting retrofitted UGI measures represent the maximum possible implementation without significant land use changes for that specific. The general placement strategy, the location (cells changed), and the type of land cover change of UGI elements implemented in the studied scenario are summarized in Table 3.

Table 2
Categorization of the grid cells of the study area based on the percentage of built-up land cover with Google Earth images for each category.

Category 1	Category 2	Category 3	Category 4
Non-urbanized >75% Non-urban ≤ 25% Urban	Sparsely urbanized 51–75% Non-urban 26–50% Urban	Urbanized 26–50% Non-urban 51–75% Urban	Highly urbanized ≤ 25% Non-urban >75% Urban
			

Table 3
Elements implemented in the UGI scenario, general placement strategy (based on (Fluhrer et al., 2021), grid cells changed for implementation and imposed land cover change for UGI implementation.

UGI element	General placement strategy	Cells changed	Land cover change (status quo to UGI)
Permeable pavement	Low-trafficked streets	51, 52, 49, 32, 41, 50, 36, 43, 48, 30, 13, 46, 24, 40, 7, 42, 19, 18, 17, 31, 28, 37, 27, 1, 5, 14	Paved to bare soil
Swale	Unbuilt space next to river	49/27 and 40/29	Paved/ bare soil to grass
Constructed wetlands	Minimum of unbuilt space of 5 ha	40, 34 and 36/26	Trees/shrubs/grass to water
Stormwater trees	Alonge streets with sufficient width and already existing trees	24, 46, 37	Paved to tree/shrub
28 bioretention cells	Min. length of 10 m, excluding driveways, max. Width of 3 m	7, 13, 24, 31, 36, 40, 43, 48, 49, 50, 51	Paved to grass
Infiltration trenches	Street curb of min. Length of 10 m	7, 15, 24, 28, 30, 31, 32, 40, 41, 43, 46, 49, 50, 51	Paved to grass

Stormwater trees were modeled by adding trees at the proposed locations into the CDSM. They were simulated by changing the roughness parameters to represent a surface type with evergreen tree/shrub. To simulate constructed wetlands, the surface type of the land cover type was set as water. Bioretention areas, swales, and infiltration trenches were modeled as a grass land cover type. Since an intermediate state between impervious and highly pervious land cover is not available in SUEWS, the permeable pavement was modeled as bare soil, thereby assuming a similar infiltration capability. For the scope of this study, this assumption simplifies the simulation, although the difference of infiltration and evaporation capacity between bare soil and permeable pavement is unknown. Suitable areas for detention- or retention basins lie in green open spaces. Changing the surface type for the simulation is not an option and consequently, this UGI measure was omitted from the study.

Fig. 4 shows the changes made to the land cover classification layer employed to model the status quo when modeling the described UGI measures. The location and dimensions of the UGI measures for the hypothetic second scenario with implemented UGI are taken from Fluhrer et al. (2021). For both model runs, for the status quo and the UGI scenario, the same driving force was used. The two model runs differ exclusively in the changes applied to the status quo described above to represent UGI implementation. Since all other model input remained the same, the difference in outputs results from the UGI implementation and was compared in relation to the status quo model outputs.

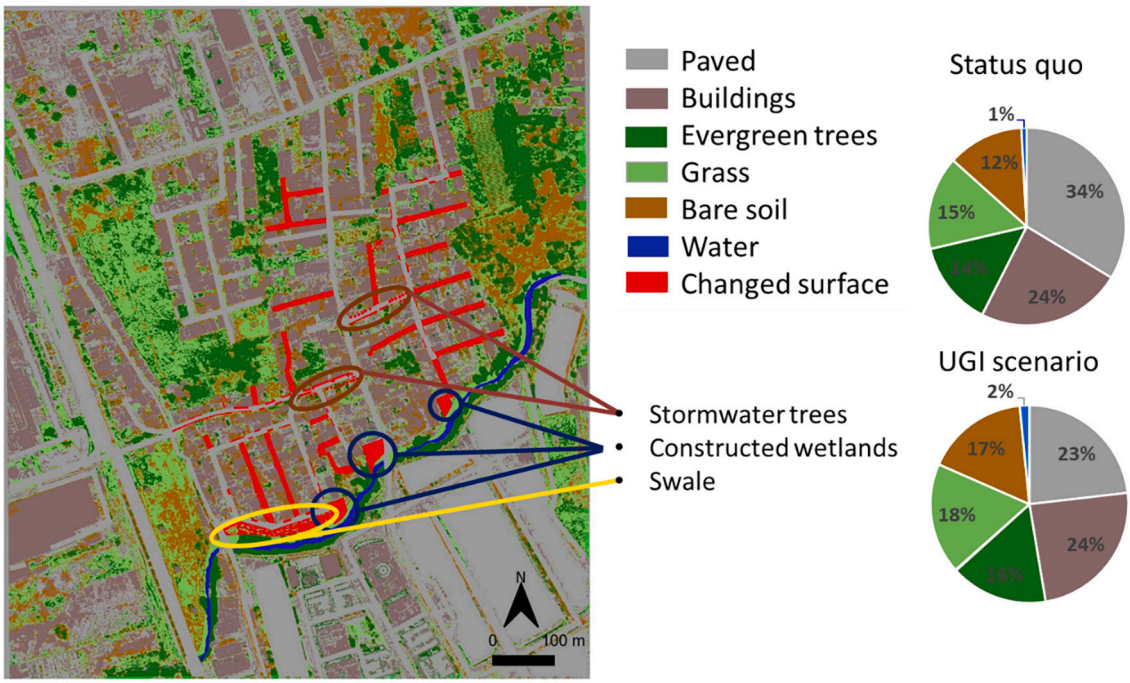

Fig. 4. Left: High resolution land cover classification of the study area indicating the location and type of surface changes applied to simulate the UGI scenario. Right: Surface fractions of the status quo and the UGI scenario.

2.4.3. Statistical, spatial, and temporal evaluation

To evaluate the model output of both scenario runs throughout the study area the average for the heat fluxes (P), were calculated based on Eq. 5, where t describes the hourly time step and i the respective cell of the grid.

$$P_i = \frac{1}{n}\sum_{t=0}^{n} P_t \tag{5}$$

The statistical evaluation describes the average spatial parameter distribution throughout the grid, represented in a boxplot (Fig. 7). The average of each parameter was calculated, primarily employing Eq. 5, and secondly employing Eq. 6, where P_{Av} is the respective averaged parameter and the initial i represents the respective cell.

$$P_{Av} = \frac{1}{n}\sum_{i=0}^{n} P_i \tag{6}$$

Additionally, to quantify the deviation between the scenarios, the variation in the percentage of the average of the grid was calculated with Eq. 7, where P describes the respective parameter of the energy balance, i is the respective cell and SQ describes the results of the status quo and UGI describes the results of the simulated UGI implementation.

$$P_{Dev} = \frac{\frac{1}{n}\left(\sum_{i=1}^{n} p_{i,SQ} - \sum_{i=1}^{n} p_{i,UGI}\right)}{\frac{1}{n}\sum_{i=1}^{n} P_{i,SQ}} \tag{7}$$

The spatial evaluation enables observations of the impact of land cover (degree of impervious surface) and punctual deviations for each cell.

For the temporal evaluation the average is calculated over each category. In Eq. 8, P_{Ca} is the respective parameter per category and P_{Cell} is the parameter of a cell, differently to Eq. 5 and 6, where P_i is the parameter per cell, after averaging over time.

$$p_{ca} = \frac{1}{n}\sum_{cell=1}^{n} p_{cell} \tag{8}$$

The Bowen Ratio (β) is a ratio of the turbulent heat fluxes Q_H/Q_E. It is calculated to evaluate which heat process dominates. If $\beta < 1$, the latent heat flux is the dominant process, keeping the air cooler by converting energy into evaporating water. The water vapor with a higher energy state liberates the energy again while condensation, mostly in the process of cloud and rain formation. Conversely, the sensible heat ($\beta > 1$) indicates that more energy is channeled to warming the lower atmosphere (Oke et al., 2017). β was used to evaluate the impact of the grid cell's degree of urbanization in the status quo and changes in the energy balance in the hypothetical UGI

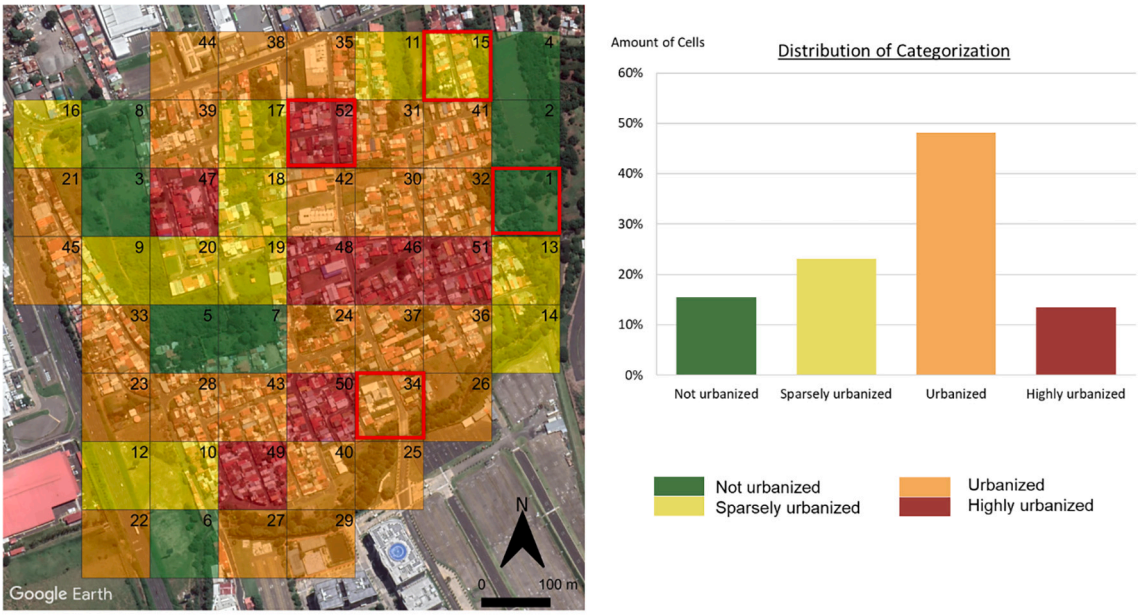

Fig. 5. Map of the study area showing the category of urbanization of each grid cell (left). Numbers in the upper right corner of each cell show the cell ID. Grid cells framed in red are representative cells for each urbanization category. On the right the proportionate distribution of each category throughout the grid is given. Source of background image: Google Earth. (For interpretation of the references to colour in this figure legend, the reader is referred to the web version of this article.)

scenario.

3. Results

3.1. Grid distribution and comparison of different degrees of urbanization

Fig. 5 shows the spatial distribution of grid cells with different degrees of urbanization obtained from the land cover classification (see section 2.4.1.). Most of the grid cells were categorized as urbanized (48%). About 13% were categorized as mostly urbanized (red), thus together more than 60% of the area was characterized by dominantly urbanized surface cover (red and orange). Moreover, most grid cells including the river corridor at the southern border were categorized as urbanized highlighting the impact of urban development on riparian areas. The remaining grid cells were categorized as not urbanized (green, 15%) or sparsely urbanized (yellow, 23%), mainly covered with pervious surfaces and vegetation. The central area was mainly composed of urbanized or highly urbanized grid cells dominated by buildings and streets with barely any vegetation. Consequently, the central grid cells present an altered water and energy balance indicated by less infiltration, higher runoff, and less evapotranspiration.

Table 4 shows the surface cover fractions for exemplary cells of each urbanization category. The six SUEWS surface cover fractions were merged into two classes, non-urban and urban, to determine the degree of urbanization. Cell 1 is the least urbanized cell, located in the east of the study area, while cell 52 is the most urbanized cell. The other categories are represented by their median cells. The described cells of Table 4 are highlighted with red frames in Fig. 5.

Based on the SUEWS modeling results, the β of each cell was calculated to quantify the impact on the latent and sensible heat fluxes of different degrees of urbanization within the study for the simulation of status quo (Fig. 6). The ratio of the turbulent heat fluxes Q_H/Q_E was calculated for each cell (Eq. 5). The result of β per cell follows the degree of urbanization. Evaporation as dominant process was found in only one cell, cell 3 (categorized as *Not urbanized*, framed with a dashed red box). For all other cells, the sensible heat flux was the dominant process. Nevertheless, Fig. 6 shows that the highest ratio (in red) were simulated in those cells that were categorized as *Highly urbanized* or are adjacent to such cells. Almost all β values of the core urbanized area exceed a value of 2.5 (in orange and red) indicating a strong urbanization impact on the energy balance. β lower than 1.5 (in green) resulted only in cells categorized as *Not* or *Sparsely urbanized*, whereas β lower than 1.0 resulted only in one cell (in light green). The highest ratio (5.56) was detected in the most urbanized cell (52) followed by a ratio of 5.44 for the second most urbanized cell (51). Of all *Not urbanized* cells, cell 1 resulted in the highest β. This could be due to the influence of the three neighboring cells to west that all have a high degree of built-up land cover and modeled β (3.59–5.44).

3.2. Comparison of status quo and UGI scenario modeling results

The statistical distribution describes the overall modeling outcomes for the study area, by representing the variety of model outputs over all cells. The analysis of the spatial distribution allows to compare the modeling output of each cell, including factors influenced by its location. The temporal distribution provides insight on temporal factors such as meteorological conditions influencing temporally the model output.

3.2.1. Statistical distribution

The time averaged statistical distribution of the model outputs for each grid cell, and which resulted from each scenario, is displayed as box plots in Fig. 7.

Regarding changes in the water balances, the results showed that the maximum averaged grid cell values for total change in water storage increased specifically for a few particular cells. The UGI scenario resulted in a higher storage capacity,with an average increase of 5% in comparison to the status quo. On average for all cells for the UGI scenario, evapotranspiration increased (+3%), while surface runoff decreased (−4%). By changing 11% of the impervious to pervious land cover, the UGI scenario resulted in a more natural water balance through increasing water storage in soils and evapotranspiration, thereby reducing surface runoff. Fig. 7 shows at the bottom the absolute results of the net storage heat flux (Q_S), sensible heat flux (Q_H) and latent heat flux (Q_E) for each cell (Eq. 5 and 6) for both scenarios.

Fig. 7 shows relatively small changes for the storage heat flux and the latent heat flux. The sensible heat flux (Q_H) diminished in the UGI case on average a 16% (Eq. 7). All statistical values for the sensible heat flux diminished from a range of 47–86 W/m^2 (status quo) to 44–73 W/m^2 (UGI). The maximum and minimum of the latent heat flux remained at a similar extent only showing a change of about 1,5 W/m^2 more (minimum and mean).

These results show that the land cover fraction conversion had an effective cooling impact in the UGI scenario. The statistical

Table 4
The surface fractions for SUEWS six surface classes and the surface fraction for the (non-)urban classes for one cell of each urban category.

Cell	Paved	Build	Ever-green	Grass	Bare soil	Water	Non-urban	Urban	**Category**
1	0.01	0	0.35	0.18	0.46	0	0.99	0.01	Not urbanized
15	0.15	0.29	0.25	0.17	0.14	0	0.56	0.44	Sparsely urbanized
34	0.33	0.30	0.09	0.13	0.13	0.02	0.37	0.63	Urbanized
52	0.33	0.50	0.02	0.04	0.11	0	0.17	0.83	Highly urbanized

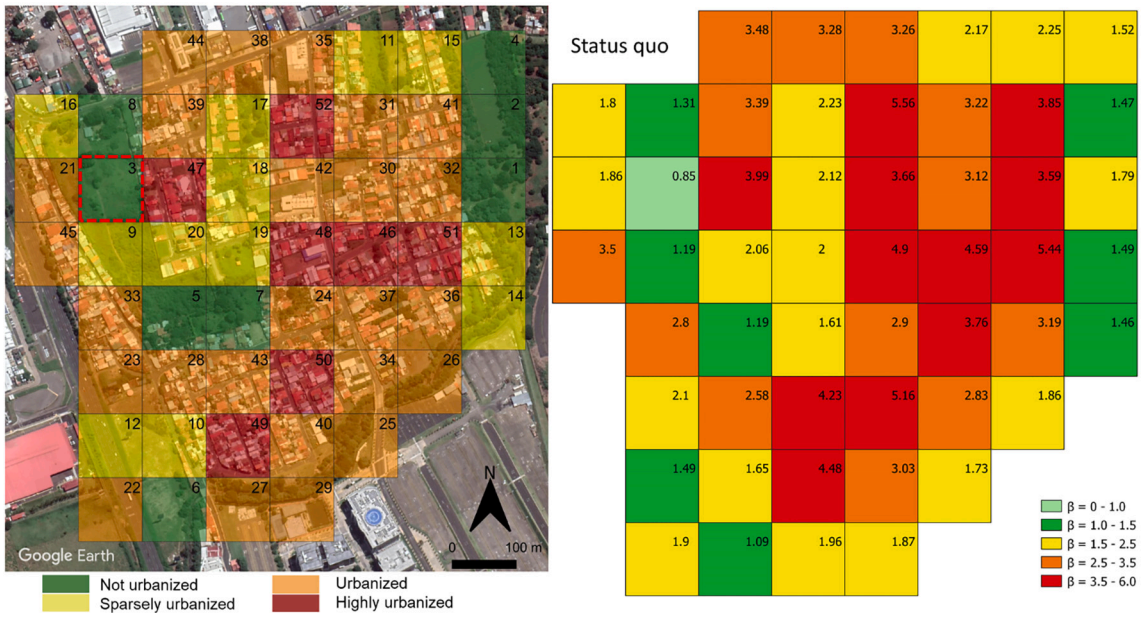

Fig. 6. The distribution of β for the status quo is given on the right (exact ß values for each cell in the upper right corner). The left image shows the urbanization categorization (colour) and cell ID. The red dashed frame highlights the only cell with evaporation as its dominating process (β <1). Source of background image: Google Earth. (For interpretation of the references to colour in this figure legend, the reader is referred to the web version of this article.)

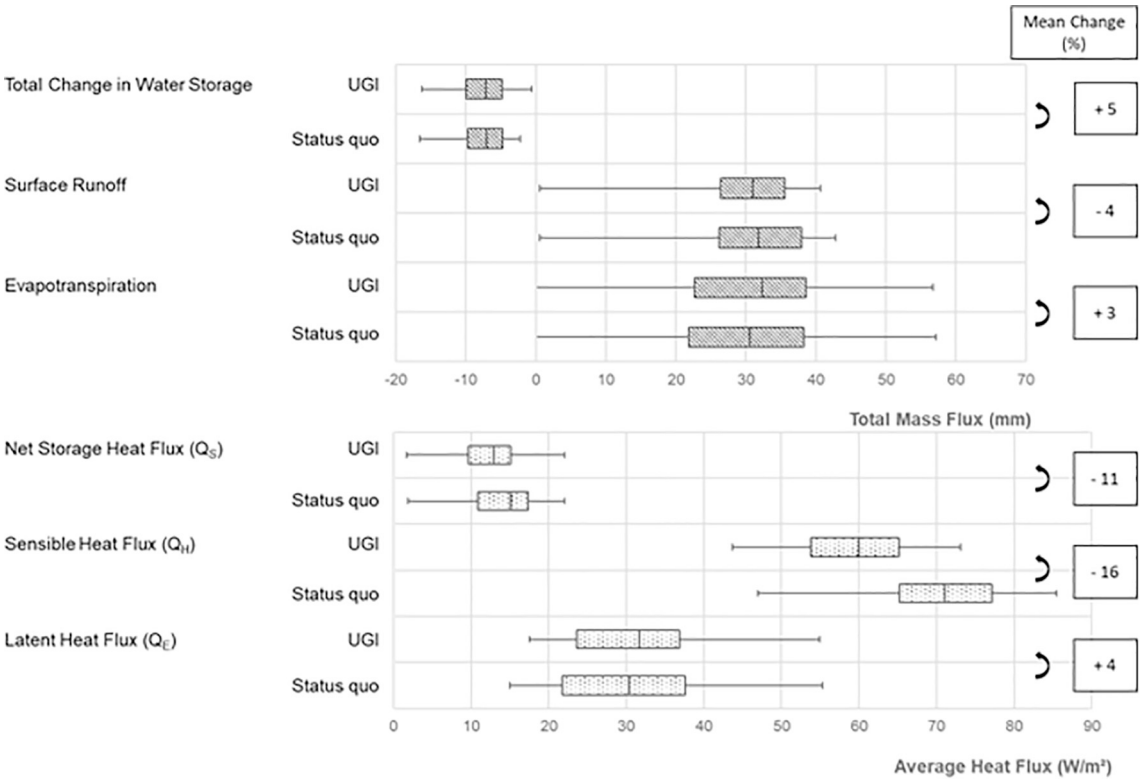

Fig. 7. Box plots showing the statistical distribution model output parameters of the water balance (top) and energy balance (bottom) of all cells of the grid, the values on the right represent the mean relative change (reference scenario: status quo).

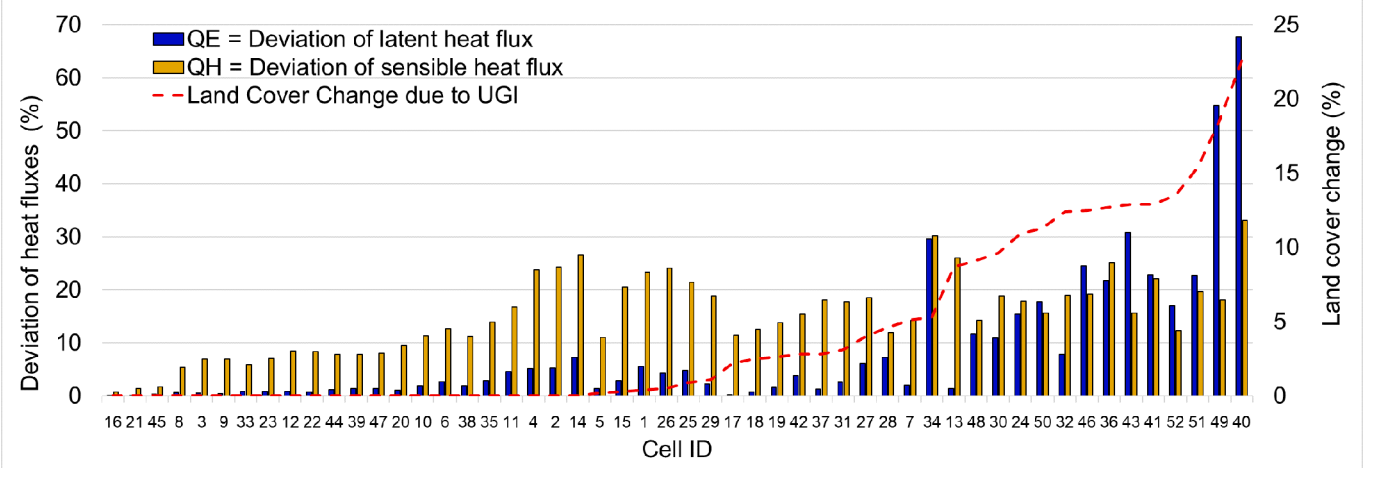

Fig. 8. Deviation of latent heat flux (blue) and sensible heat flux (yellow) between the status quo and the implemented GI scenario per cell, sorted by percentage of land cover change. The land cover change (red dashed line) indicates the changes made for the UGI scenario for each cell. (For interpretation of the references to colour in this figure legend, the reader is referred to the web version of this article.)

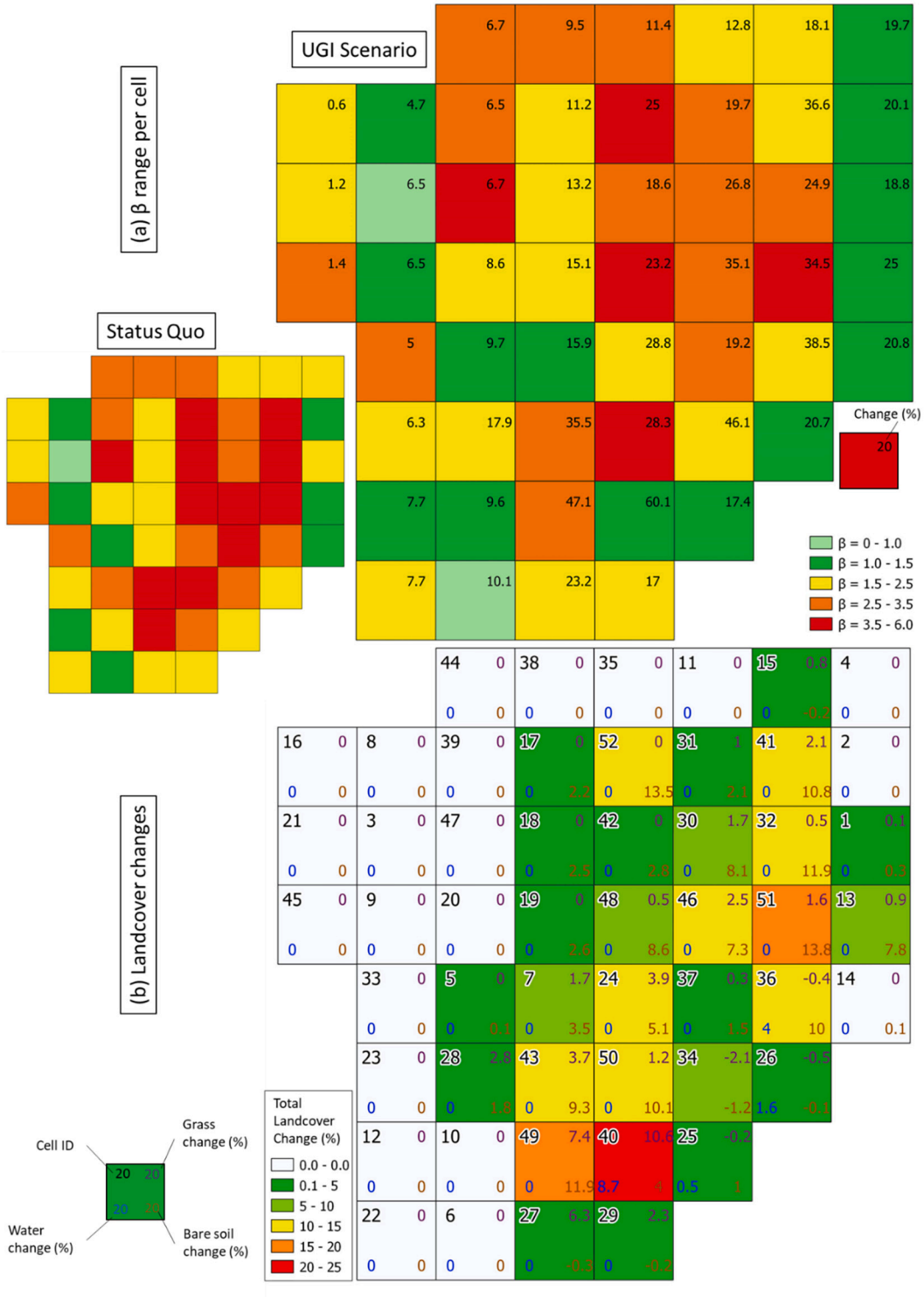

Fig. 9. (a) Range of β per cell: the colour-coding of each cell indicates the resulting value range of β for status quo (left) and UGI scenario (right). The values show the respective change in β. (b) Land cover changes for each cell.

distributions of averaged grid cell model outputs provided general insights on the potential impact of UGI induced land cover conversion. Therefore, the location and which specific factors influenced those changes remains unclear.

3.2.2. Spatial distribution

To reveal the spatial impact of the land cover fraction conversion in the UGI scenario, the relative difference between the status quo and the UGI scenario (deviation) was calculated for each grid cell and process (i.e. Q_E and Q_H) and averaged over time (Eq. 7). In Fig. 8 the cells (x-axis) are sorted by their total land cover change representing the simulated UGI implementation. The dashed red line indicates the relative land cover change per cell. From cell 16 until cell 14 no land cover was changed and until cell 26 land cover changes are ≤0,5%). Nevertheless, the sensible heat flux (Q_H in yellow) deviated from the status quo by up to 26% (Cell 14). Throughout the grid, the deviation of Q_H for changed cells varied between 15 and 33%. The latent heat flux (Q_E in blue) showed deviations in the unchanged cells by up to 7%. For Q_E the results varied significantly between the cells. This result is not related to the land cover change within the cells. For instance, cell 34 shows a deviation of 30%, while cell 13 deviates by 1% although the land cover change is higher. The highest deviations for Q_E were found in cells 49 (54%) and 40 (68%).

Fig. 8 shows that changes in land cover influenced the heat fluxes. Even surrounding cells, in which no land cover change was implemented, showed an impact in the energy balance, especially for the sensible heat flux. For example, cells 11, 4, 2, and 14 showed a change in latent (more than 5%) and sensible heat flux (more than 15%), although no change in the parameterization occurred. Moreover, the neighboring cells also changed, which suggests that themodel outputs in the unchanged cells are were also influenced. This change can be observed in cell 14. The land use was changed in four neighboring cells, including two cells increasing water fractions (cell 36 by 4% and cell 26 by 1.6%).

Fig. 9 shows at the bottom the percentage of land cover changed for each cell between scenarios and on top with a colour code the β values and like numbers in the cells, the relative changes (%) in β per cell for the UGI scenario compared to the status quo β (displayed on the left). Underneath the figure, the cell IDs are placed in the left, upper corner, and the green number represents a change into grass, as either bioretention area or infiltration trench. The highest change occuredin cell 49 with +7.9%, and cell 40 with +10.6%. The blue number represents the percentage changed into water, as constructed wetlands, mostly in cells 40 and 34. The brown number represents the percentage of land cover changed into bare soil as permeable pavements. The colour of each square illustrates the percentage changed from urban to non-urban land cover classes (i.e. the percentage of total UGI implementation), while the white cells were not modified.

When combining the information out of Figs. 8 and 9, the following results became visible. The highest deviation of Q_H (> 30%) was obtained in cells 40 and 34, where surface changed mostly into water to represent the constructed wetlands in the UGI scenario. The highest deviations of Q_E (> 50%) was found in cells 40 and 49, which experienced the highest total land cover change in the UGI scenario. Cells 40 and 49 had the highest change for β (60.1% and 47.1, see upper part (a) of Fig. 9), cell 34 has the third-highest change (46.1%).

The value β approximates 1 when the sensible heat flux diminishes while the latent heat flux rises. As Fig. 9 shows, implementing UGI in only certain cells changed the turbulent fluxes for all cells of the grid. Cells in the center simulating UGI had the highest reduction of β (20–60%). β was reduced by 10% in cell 6 – showing that the latent heat flux is the dominative heat flux (β < 1). All cells in the two columns in the east presented changes in β < 8%. Those are the cells farthest away from cells with land use changes. However, cells in the western boundary column experienced a change in β around 20% or more, although only one cell was significantly affected by a land cover change (cell 60).

In consequence, implementing green areas, green swales, or similar, can lead to a shift in the energy balance from sensible to latent heat fluxes. Modeling an increase of the percentage of greenspace from 48% to 53% resulted in a decrease from 2.7 to 2.1 in average.

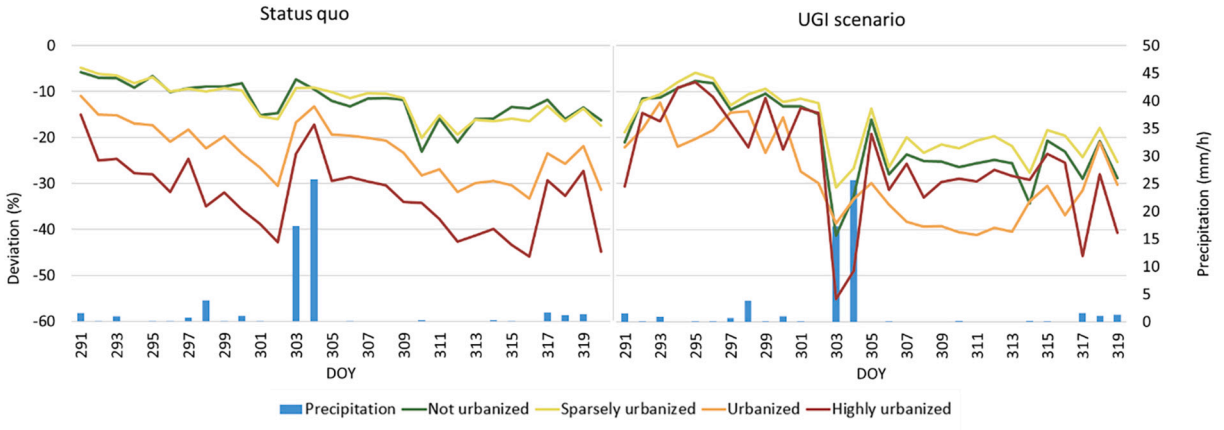

Fig. 10. Relative deviation of the Bowen Ratio (β) over time, averaged over cells for each category: not urbanized (green), sparsely urbanized (yellow), urbanized (orange) and highly urbanized (red), and the bars in blue show the hourly precipitation of the status quo (left graph) and UGI scenario (right graph). (For interpretation of the references to colour in this figure legend, the reader is referred to the web version of this article.)

Cells with a $\beta < 1.5$ (green and light green cells in Fig. 9) increased by seven, and cells with a $\beta > 3.5$ was reduced by seven.

3.2.3. Temporal distribution

The temporal distribution for each modeled output was also influenced by meteorological factors such as precipitation, temperature, and wind speed. Results showed that an increase in evaporation lead to an increase of latent heat fluxes following rain events, providing water to evaporate. Additionally, the energy balance was dependent on solar radiation, therefore the heat fluxes during the day are higher than during the night.

The wind speed used for both scenarios lies in a range of 0.01 m/s to 2 m/s. The average diurnal wind speed of the study period was 0.8 m/s and the nocturnal wind speed 0.6 m/s. The precipitation of the study period is presented in Fig. 10. The main rain occasion was modeled for the Day of the year (DOY) 303 and 304.

Fig. 10 shows that β was reduced for both, diurnal and nocturnal heat fluxes. Each graph of the figure includes four lines, representing an average of all cells per urbanization category (Eq. 8). While the diurnal β of not-urbanized cells lies in a range of $\beta = 0.4$–2 the range of highly urbanized cells was $\beta = 0.8$–10.4. The diurnal deviation between the scenarios was reduced to 46% from 10.4 to 5.6. However, β diminished during rain. The diurnal β deviations continuously increased during dry periods, mostly for the urbanized and highly urbanized cells, and rapidly decrease when rain occurred. The higher the degree of urbanization of cells, the stronger the β increased in the UGI scenario due to rain.

The nocturnal β presented a similar range between 0.6 and 20 for each urbanization category. Both absolute values of the heat fluxes were lower during the night (maximal 38 W/m^2). Due to occasionally low latent heat fluxes during the night ($Q_{E,min} = 1.3$ W/m^2), β reached these high values. Fig. 10 also shows that the ratio of the nocturnal deviation decreased for the whole period, reaching its maximal reduction during the main rain event. The increasing trend of β deviations during dry periods cannot be observed in the nocturnal β deviations.

4. Discussion

The use of surface models to simulate climatic effects has the great advantage that they can be applied in environments outside the area in which they have been developed and evaluated (Alexander et al., 2015). Especially applications to rapidly growing cities in the economically developing world, as in the case of this study, the results of such models may have greatest impact with regard to informing planning decisions. But particularly for more complex urban models, data requirements can represent a major obstacle to their employment. If available in an ideal case, measurements of flux towers can be used to provide model input and to evaluate the models simulations of turbulent fluxes in detail (Roth et al., 2017). In this study, standard meteorological data was used with satisfactory results. Alexander et al. (2015) compared the performance of SUEWS when using flux tower or standard meteorological data and came to the conclusion that both kinds of model inputs lead to similar results. Hence, suggesting that the SUEWS model can be used with data that is more easily derived, i.e. standard meteorological data as in this study. Their comparison also showed the importance of including vegetative cover and of the initial moisture state in simulating the urban energy budget. Here, the use of land cover information of high spatial resolution and the definition of the initial soil moisture state based on in-situ measurements in this study were beneficial to produce more reliable results. Although soil moisture measurements may not be available at other sites, the use of standard meteorological data in combination with high resolution land cover information obtained from freely available data enables the application of SUEWS to model urban climatic effects and UGI in less developed regions of the world.

In this study, a high-resolution grid of 100 × 100 m was used as an approach to include small-scale characteristics of the urban fabric and to assess the impact of distributed UGI implementation. This high resolution represents a novel approach as the model has so far mainly been used with grids of lower resolution (least grid cell size 400 × 400 m according to the model developers). The 100 × 100 m grid cell size model used in this study generated plausible results and demonstrated significant potential for simulating small scale urban characteristics and UGI.

Typical modeling outputs resulted for each cell of the grid, following the degree of urbanization, classified by surface fractions, e.g., Bowen Ratios are higher where cells represent urbanized areas. Literature values of Bowen Ratios for urban areas with 35–75% (in this study sparsely urbanized), 20–35% (urbanized), and < 20% (highly urbanized) greenspace range between 0.5 and 2.5, 1.5–3, and 3–8 respectively (Oke et al. 2017). The results of this study show similar Bowen Ratios for the different urbanization degrees (Fig. 6). The lowering effect of the Bowen Ratio due to the surface fraction changes through the UGI implementation seems in the light of the given literature values plausible. The simulation of constructed wetlands as water surface fractions appears to be justified when looking at the Bowen Ratios for wetlands (0.2–0.7) which are similar to those of lakes (0.2–1) and the resulting lowering effect of the Bowen Ratio in the UGI scenario. This shows that SUEWS has the potential of modeling complex effects such as the urban heat island at the scale considered in this study.

When increasing natural surfaces, such as vegetation and water, the general trend is towards a reduction of the sensible heat flux while the latent heat flux is increased (Roth et al., 2017). However, in this study, this effect not only occured in modified cells but over the whole grid. The potential of SUEWS for showing the impact of UGI across an urban landscape (i.e. beyond the site of implementation) needs further research regarding effect of β during longer periods of time toassess seasonal effects, and adjusted radiative properties (albedo, emissivity). This could be of special interest for policy-makers and landscape planners, especially in showing how UGI not only influences locally but in a larger area.

Moreover, the effect of the population density required its impact on the energy and water balance is suggested in future studies. The individual grid cell's population density could be better estimated by relating population density to the relative share of the building class in each cell since this information is available from the land cover classification at a high-resolution. This way a more

realistic and detailed influence of the anthropogenic heating or cooling could be taken into account.

Representing UGI elements in cells of SUEWS as changes in surface cover fractions (land cover) in the way it was done in this study is therefore an approximation to the impact of UGI elements that is not without flaws.

The modeling assumption about permeable pavement represented as baresoil resulted in an increase of infiltration and evaporative capacity, but not necessarily of the same magnitude that actual permeant pavement. The degree of permeability and moisture storage characteristics of permeable pavement are more difficult to represent in the model. Thus, the actual behavior of permeable pavement could be different. Compared to the other UGI representations through surface fractions (land cover), the difference between permeable pavement and bare soil regarding surface texture and albedo is likely greater, potentially representing the greatest source of bias with energy exchanges.

Swales were introduced as a surface fraction change from paved or bare soil to grass representing vegetated swales. In case of a change from paved to grass, the additional effect in infiltration and evapotranspiration in exchange of surface runoff seems reasonable. In case of bare soil to grass, the additional effect of transpiration through grass seams is also reasonable. However, the storage characteristics could be different as the drainage of swales could not be considered.

The surface fractions of trees, shrubs, or grass were changed from water to simulate constructed wetlands. This resulted in a reasonable increase in evaporation for the water surface, but the plant transpiration, as well as storage and retention function of surface runoff from upstream connected cells, could not be represented in SUEWS.

Stormwater trees were simulated as a surface fraction change from paved to trees. The resulting additional effects of increased infiltration and evapotranspiration in exchange of surface runoff are generally reasonable. However, storage and retention functions of surface runoff from upstream connected cells could not be represented in SUEWS. A similar case is the model representations of bioretention cells and infiltration trenches as a surface change from paved to grass where the effect of increased infiltration and evapotranspiration in exchange of surface runoff appears reasonable while storage and retention of surface runoff from upstream connected cells could not be represented.

In general, all UGI elements could probably store more water subsurface and thereby increase evapotranspiration through higher availability of water than their surface fraction representation in SUEWS can. Thus, evapotranspiration from UGI elements could be higher and therefore surface runoff and/or infiltration lower. This could also result in a different energy balance, implying an even higher reduction of the sensible heat flux and in turn an increased latent heat flux.

To summarize, SUEWS allows for a more detailed water and energy balance modeling regarding the changes of surface characteristics of cells, but it cannot represent specific hydraulic characteristics resulting from a specific technical design of UGI elements which are important for the representation of surface runoff flow, storage, and conveyance to the outfalls of an area. SUEWS enables one to estimate the UGI impact across space (i.e. how heat fluxes change and are influenced across cells). This is due to the distributed model structure (grid cells) and the detailed model representations of aerodynamic exchange. The representation of urban evapotranspiration at a fine timescale enables SUEWS to estimate urban evapotranspiration under all conditions (Grimmond and Oke, 1991), in particular during and immediately following rain when impervious surfaces are wet and water is lost through evaporation and runoff. This is an additional advantage of SUEWS compared to commonly used urban hydrological simulation models (Mitchell et al., 2008) when assessing the impact of UGI on local (house and street level) and regional (neighborhood) heat fluxes (e.g. to estimate Urban Heat Island Impact).

Mitchell et al. (2008) used an earlier version of SUEWS, the SUES model, to demonstrate the impact of a range of water sensitive urban design strategies on water exchanges and to reveal from the energy balance how these designs would affect air temperature. They modeled wetlands as water bodies as it was done in this study, but they modeled lined grassed swales as a shallow soil store (100 mm capacity), with wetting losses only, i.e. no exfiltration; and vegetated roof as a shallow soil store with 10 mm capacity. Contrary to this study, in the cases of swales and vegetated roofs (not considered in this study), Mitchell et al. (2008) modified the subsurface properties to model the infiltration and storage functioning of these UGI elements.

The simulation of the UGI scenario in this study represented a reduction of paved areas (−11%) and an increase in vegetated (+5%), water (+1%), and permeable areas (+5%). This resulted in a heat storage reduction (averaged over time and all cells) of 11%. This result is of similar magnitude to modeling results of low impact development design interventions for the city of Dublin (Alexander et al., 2016) where paved areas where replace (−10%) by grass (+5%) and trees (+5%). Compared to the original state, this resulted in a reduction of heat storage of 7.9%. The higher reduction in our case could be explained by the tropical climate resulting in higher heat fluxes.

Urban land surface models (ULSM) such as SUEWS have mostly been evaluated and optimized for mid- and high-latitude cities (Demuzere et al., 2017). However, in a comparative evaluation of four ULSMs, including SUEWS, for a tropical residential neighborhood in Singapore overall results indicated good model performance for most energy balance components. The simulation results of all models aligned well with previous findings for mid-latitude regions, suggesting a principal transferability of these models to tropical regions. In the study of Demuzere et al. (2017), a specific sensitivity of the latent heat flux directly after a precipitation event resulting a positive bias was detected. This effect is also mirrored in this study's results and specifically pronounced in the UGI scenario when permeable surfaces were increased. This shows the need to investigate further in specific weather conditions.

5. Conclusions

Land cover change due to urbanization has a strong impact on the water and energy balance. In complex urban fabrics, even small patches of water, vegetation, or unsealed surfaces can make a difference. Employing the software SUEWS, this study showed the modeling varying response of grid cells according to different degrees of urbanization. The runoff reducing, infiltration, and

evapotranspiration increasing effect as well as the lower β values of less urbanized cells were shown. The effects on the energy balance are not limited to the cell level but extend across other cells. Additionally, changes in the water and energy balance resulting from the implementation of Urban Green Infrastructures were also assessed regarding the regulating effects of the local and regional energy balance resulting in micro-climate regulation. UGI can provide a variety of benefits to society and the environment. UGI benefits regarding surface runoff control and water treatment have been widely acknowledged in science, and implementations in practice have shown their effectiveness. The model was set up using a high-resolution land cover classification and a grid size of 100 × 100 m enabling a spatially explicit discretization of UGI elements along and within streets as well as at open spaces in a densely urbanized residential area at sites identified as suitable for stormwater control during fieldwork.

This study demonstrated that SUEWS enables a detailed simulation of different degrees of urbanization and spatial placement of retroffited UGI elements at a neighborhood scale. A complementary or combined use of both types of models to grasp the broad benefits of implementing UGI in densely urbanized to a fuller extend is suggested. This kind of application should be further investigated.

Declaration of Competing Interest

The authors declare that they have no known competing financial interests or personal relationships that could have appeared to influence the work reported in this paper.

Acknowledgements

This research was funded by the German Federal Ministry of Education and Research (BMBF), grant number 01UU1704.

Appendix

Table A.1
Total fractions for each surface cover layer of the status quo and the UGI scenario.

Surface Cover (Total Fractions)	Status quo	UGI scenario
Paved	0.34	0.23
Buildings	0.24	0.24
Evergreen Tree/shrubs	0.14	0.16
Deciduous Tree/shrubs	0.00	0.00
Grass	0.15	0.18
Bare Soil	0.12	0.17
Water	0.01	0.02

References

Ahiablame, L.M., Engel, B.A., Chaubey, I., 2012. Effectiveness of low impact development practices: literature review and suggestions for future research. Water Air Soil Pollut. 223, 4253–4273. https://doi.org/10.1007/s11270-012-1189-2.

Alexander, P.J., Mills, G., Fealy, R., 2015. Using LCZ data to run an urban energy balance model. Urban Clim. 13, 14–37. https://doi.org/10.1016/j.uclim.2015.05.001.

Alexander, P.J., Fealy, R., Mills, G.M., 2016. Simulating the impact of urban development pathways on the local climate: a scenario-based analysis in the greater Dublin region. Ireland. Landsc. Urban Plan. 152, 72–89. https://doi.org/10.1016/j.landurbplan.2016.02.006.

Chapa, F., Hariharan, S., Hack, J., 2019. A new approach to high-resolution urban land use classification using open access software and true color satellite images. Sustainability 11, 5266. https://doi.org/10.3390/su11195266.

Chapa, F., Pérez, M., Hack, J., 2020. Experimenting transition to sustainable urban drainage systems—identifying constraints and unintended processes in a tropical highly urbanized watershed. Water 12, 3554. https://doi.org/10.3390/w12123554.

Chen, V., Bonilla Brenes, J.R., Chapa, F., Hack, J., 2021. Development and modelling of realistic retrofitted nature-based solution scenarios to reduce flood occurrence at the catchment scale. Ambio. https://doi.org/10.1007/s13280-020-01493-8.

Chui, T.F.M., Liu, X., Zhan, W., 2016. Assessing cost-effectiveness of specific LID practice designs in response to large storm events. J. Hydrol. 533, 353–364. https://doi.org/10.1016/j.jhydrol.2015.12.011.

Communities, European, 2001. Towards a Local Sustainability Profile. European Common Indicators. Methodology Sheets. Luxembourg.

Curridabat, M.D.E., 2021. Guía de Plantas Dulces.

Demuzere, M., Harshan, S., Järvi, L., Roth, M., Grimmond, C.S.B., Masson, V., Oleson, K.W., Velasco, E., Wouters, H., 2017. Impact of urban canopy models and external parameters on the modelled urban energy balance in a tropical city. Q. J. R. Meteorol. Soc. 143, 1581–1596. https://doi.org/10.1002/qj.3028.

Dietz, M.E., 2007. Low impact development practices: a review of current research and recommendations for future directions. Water Air Soil Pollut. 186, 351–363. https://doi.org/10.1007/s11270-007-9484-z.

Dietz, M.E., Clausen, J.C., 2008. Stormwater runoff and export changes with development in a traditional and low impact subdivision. J. Environ. Manag. 87, 560–566. https://doi.org/10.1016/j.jenvman.2007.03.026.

Elliott, A., Trowsdale, S., 2007. A review of models for low impact urban stormwater drainage. Environ. Model. Softw. 22, 394–405. https://doi.org/10.1016/j.envsoft.2005.12.005.

EPA, 2020. What Is Green Infrastructure? [WWW Document]. Webpage Green Infrastruct. Progr. United States Environmetal Prot. Agency. URL. https://www.epa.gov/green-infrastructure/what-green-infrastructure (accessed 4.23.20).

European Commission, 2013. Communication from the commission to the european parliament, the council, the european economic and social committee and the committee of the regions: Green Infrastructure (GI) — Enhancing Europe's Natural Capital. Brussels, Belgium.
Fletcher, T.D., Shuster, W., Hunt, W.F., Ashley, R., Butler, D., Arthur, S., Trowsdale, S., Barraud, S., Semadeni-Davies, A., Bertrand-Krajewski, J.-L., Mikkelsen, P.S., Rivard, G., Uhl, M., Dagenais, D., Viklander, M., 2015. SUDS, LID, BMPs, WSUD and more – The evolution and application of terminology surrounding urban drainage. Urban Water J. 12, 525–542. https://doi.org/10.1080/1573062X.2014.916314.
Fluhrer, T., Chapa, F., Hack, J., 2021. A methodology for assessing the implementation potential for retrofitted and multifunctional urban Green infrastructure in public areas of the global south. Sustainability 13, 384. https://doi.org/10.3390/su13010384.
Göbel, P., Stubbe, H., Weinert, M., Zimmermann, J., Fach, S., Dierkes, C., Kories, H., Messer, J., Mertsch, V., Geiger, W.F., Coldewey, W.G., 2004. Near-natural stormwater management and its effects on the water budget and groundwater surface in urban areas taking account of the hydrogeological conditions. J. Hydrol. 299, 267–283. https://doi.org/10.1016/j.jhydrol.2004.08.013.
Green, W.H., Ampt, G.A., 1911. Studies on soil physics, 1, The flow of air and water through soils. J. Agric. Sci. 4, 11–24.
Grimmond, C.S.B., 1998. Heat storage in urban areas: local-scale observations and evaluation of a simple model. J. Appl. Meteorol. 38 https://doi.org/10.1061/9780784480915.291.
Grimmond, P.S., 2020. SUEWS Documentation.
Grimmond, C.S.B., Oke, T.R., 1991. An evapotranspiration-interception model for urban areas. Water Resour. Res. 27, 1739–1755. https://doi.org/10.1029/91WR00557.
Grimmond, C.S.B., Oke, T.R., Steyn, D.G., 1986. Urban Water Balance: 1. A model for daily totals. Water Resour. Res. 22, 1397–1403. https://doi.org/10.1029/WR022i010p01397.
Grimmond, C.S.B., Cleugh, H.A., Oke, T.R., 1991. An objective urban heat storage model and its comparison with other schemes. Atmos. EnvironPart B, Urban Atmos. 25, 311–326. https://doi.org/10.1016/0957-1272(91)90003-W.
Hansen, R., Olafsson, A.S., van der Jagt, A.P.N., Rall, E., Pauleit, S., 2019. Planning multifunctional green infrastructure for compact cities: what is the state of practice? Ecol. Indic. 96, 99–110. https://doi.org/10.1016/j.ecolind.2017.09.042.
INEC, 2020. Estimaciones y proyecciones de Población, 2011–2050 [WWW Document].
Järvi, L., Grimmond, C.S.B., Christen, A., 2011. The surface urban energy and water balance scheme (SUEWS): evaluation in Los Angeles and Vancouver. J. Hydrol. 411, 219–237. https://doi.org/10.1016/j.jhydrol.2011.10.001.
Jayasooriya, V.M., Ng, A.W.M., 2014. Tools for modeling of Stormwater management and economics of Green infrastructure practices: a review. Water Air Soil Pollut. 225, 2055. https://doi.org/10.1007/s11270-014-2055-1.
Joyce, J., Chang, N.-B., Harji, R., Ruppert, T., Imen, S., 2017. Developing a multi-scale modeling system for resilience assessment of green-grey drainage infrastructures under climate change and sea level rise impact. Environ. Model. Softw. 90, 1–26. https://doi.org/10.1016/j.envsoft.2016.11.026.
Juan, A., Hughes, C., Fang, Z., Bedient, P., 2017. Hydrologic performance of watershed-scale low-impact development in a high-intensity rainfall region. J. Irrig. Drain. Eng. 143, 04016083 https://doi.org/10.1061/(ASCE)IR.1943-4774.0001141.
Kaykhosravi, S., Khan, U., Jadidi, A., 2018. A comprehensive review of low impact development models for research, conceptual, preliminary and detailed design applications. Water 10, 1541. https://doi.org/10.3390/w10111541.
Ketabchy, M., Sample, D.J., Wynn-Thompson, T., Yazdi, M.N., 2019. Simulation of watershed-scale practices for mitigating stream thermal pollution due to urbanization. Sci. Total Environ. 671, 215–231. https://doi.org/10.1016/j.scitotenv.2019.03.248.
Kokkonen, T.V., Grimmond, S., Murto, S., Liu, H., Sundström, A.-M., Järvi, L., 2019. Simulation of the radiative effect of haze on the urban hydrological cycle using reanalysis data in Beijing. Atmos. Chem. Phys. 19, 7001–7017. https://doi.org/10.5194/acp-19-7001-2019.
Kumar, P., Debele, S.E., Sahani, J., Rawat, N., Marti-Cardona, B., Alfieri, S.M., Basu, B., Basu, A.S., Bowyer, P., Charizopoulos, N., Gallotti, G., Jaakko, J., Leo, L.S., Loupis, M., Menenti, M., Mickovski, S.B., Mun, S.-J., Gonzalez-Ollauri, A., Pfeiffer, J., Pilla, F., Pröll, J., Rutzinger, M., Santo, M.A., Sannigrahi, S., Spyrou, C., Tuomenvirta, H., Zieher, T., 2021. Nature-based solutions efficiency evaluation against natural hazards: modelling methods, advantages and limitations. Sci. Total Environ. 784, 147058. https://doi.org/10.1016/j.scitotenv.2021.147058.
Li, Q., Wang, F., Yu, Y., Huang, Z., Li, M., Guan, Y., 2019. Comprehensive performance evaluation of LID practices for the sponge city construction: a case study in Guangxi, China. J. Environ. Manag. 231, 10–20. https://doi.org/10.1016/j.jenvman.2018.10.024.
Lindberg, F., Grimmond, C.S.B., Gabey, A., Huang, B., Kent, C.W., Sun, T., Theeuwes, N.E., Järvi, L., Ward, H.C., Capel-Timms, I., Chang, Y., Jonsson, P., Krave, N., Liu, D., Meyer, D., Olofson, K.F.G., Tan, J., Wästberg, D., Xue, L., Zhang, Z., 2018a. Urban multi-scale environmental predictor (UMEP): an integrated tool for city-based climate services. Environ. Model. Softw. 99, 70–87. https://doi.org/10.1016/j.envsoft.2017.09.020.
Lindberg, F., Sun, T., Grimmond, S., Tang, Y., 2018b. UMEP Manual Documentation.
Loridan, T., Grimmond, C.S.B., Offerle, B.D., Young, D.T., Smith, T.E.L., Järvi, L., Lindberg, F., 2011. Local-scale urban meteorological parameterization scheme (LUMPS): longwave radiation parameterization and seasonality-related developments. J. Appl. Meteorol. Climatol. 50, 185–202. https://doi.org/10.1175/2010JAMC2474.1.
Luan, B., Yin, R., Xu, P., Wang, X., Yang, X., Zhang, L., Tang, X., 2019. Evaluating Green Stormwater infrastructure strategies efficiencies in a rapidly urbanizing catchment using SWMM-based TOPSIS. J. Clean. Prod. 223, 680–691. https://doi.org/10.1016/j.jclepro.2019.03.028.
Meerow, S., 2020. The politics of multifunctional green infrastructure planning in new York City. Cities 100, 102621. https://doi.org/10.1016/j.cities.2020.102621.
Mitchell, V.G., Cleugh, H.A., Grimmond, C.S.B., Xu, J., 2008. Linking urban water balance and energy balance models to analyse urban design options. Hydrol. Process. 22, 2891–2900. https://doi.org/10.1002/hyp.6868.
Neumann, V.A., Hack, J., 2019. A methodology of policy assessment at the municipal level: Costa Rica's readiness for the implementation of nature-based-solutions for urban Stormwater management. Sustainability 12, 230. https://doi.org/10.3390/su12010230.
Offerle, B., Grimmond, C.S.B., Oke, T.R., 2003. Parameterization of net all-wave radiation for urban areas. J. Appl. Meteorol. 42, 1157–1173. https://doi.org/10.1175/1520-0450(2003)042<1157:PONARF>2.0.CO;2.
Oke, T.R., 1978. Boundary layer climates, 2nd ed.
Oke, T.R., University of B.C, Mills, G., Christen, A., Voogt, J.A., 2017. Urban Climates.
Pérez Rubi, M., Hack, J., 2021. Co-design of experimental nature-based solutions for decentralized dry-weather runoff treatment retrofitted in a densely urbanized area in Central America. Ambio. https://doi.org/10.1007/s13280-020-01457-y.
Roth, M., Jansson, C., Velasco, E., 2017. Multi-year energy balance and carbon dioxide fluxes over a residential neighbourhood in a tropical city. Int. J. Climatol. 37, 2679–2698. https://doi.org/10.1002/joc.4873.
Sailor, D.J., Vasireddy, C., 2006. Correcting aggregate energy consumption data to account for variability in local weather. Environ. Model. Softw. 21, 733–738. https://doi.org/10.1016/j.envsoft.2005.08.001.
Stewart, R.D., Lee, J.G., Shuster, W.D., Darner, R.A., 2017. Modelling hydrological response to a fully-monitored urban bioretention cell. Hydrol. Process. 31, 4626–4638. https://doi.org/10.1002/hyp.11386.
Sun, T., Grimmond, S., 2019. A Python-enhanced urban land surface model SuPy (SUEWS in Python, v2019.2): development, deployment and demonstration. Geosci. Model Dev. 12, 2781–2795. https://doi.org/10.5194/gmd-12-2781-2019.
Towsif Khan, S., Chapa, F., Hack, J., 2020. Highly resolved rainfall-runoff simulation of retrofitted Green Stormwater infrastructure at the Micro-watershed scale. Land 9, 339. https://doi.org/10.3390/land9090339.
Ward, H.C., Kotthaus, S., Järvi, L., Grimmond, C.S.B., 2016. Surface urban energy and water balance scheme (SUEWS): development and evaluation at two UK sites. Urban Clim. 18, 1–32. https://doi.org/10.1016/j.uclim.2016.05.001.
Zhang, K., Chui, T.F.M., 2017. Evaluating hydrologic performance of bioretention cells in shallow groundwater. Hydrol. Process. 31, 4122–4135. https://doi.org/10.1002/hyp.11308.